Helicopter Rotor Load Prediction Using a Geometrically Exact Beam Theory with Multibody Dynamics

S R Viswamurthy, Sang Chul Park and SangJoon Shin
School of Mechanical and Aerospace Engineering
Seoul National University, Korea

1. Introduction

Helicopters usually operate in many different conditions and perform some extreme maneuvers. Prediction of loads is therefore important for the design of the rotor system components. Helicopter blades are usually long and slender and undergo moderate to large deformations under the application of aerodynamic loads. Also, the aerodynamic environment around the rotor is highly unsteady and complex. Accurate prediction of blade and hub loads, therefore, requires an accurate aeroelastic model of the helicopter. In this paper, we attempt to develop an accurate structural dynamic model of the rotor system which can then be coupled with various aerodynamic models ranging from simple lifting line theory to CFD models to obtain the complete aeroelastic model of the helicopter.

Taking advantage of the slenderness of the rotor blade, a complex three-dimensional structural analysis problem is separated into a set of two analyses: a linear analysis over the cross-section and a nonlinear analysis of the resulting beam reference axis. In this paper, an approach based on the variational asymptotic method (VAM) [1] considering the effects of curvature, twist and warping is used to obtain the cross-sectional stiffness properties of anisotropic rotor blades. The elastic properties thus obtained are then used in a suitable one-dimensional beam analysis to obtain the axial, bending and torsional deformation of the rotor blade reference axis. The analysis in the present paper is based on an intrinsic formulation of moving beams derived by Hodges [2] and implemented by Shang and Hodges [3, 4].

2. Geometrically exact beam theory

The nonlinear intrinsic formulation originally developed by Hodges [2] assumes small strains and finite rotations. It is applicable for slender beams like helicopter blades that are initially curved and twisted. Unlike previous work, this formulation does not approximate the geometry of the deformed beam reference line and is therefore suitable for cases of large deformations.

The variational formulation was derived from Hamilton's principle which can be written as:

$$\int_{t_1}^{t_2}\int_{0}^{l}\left[d\left(K-U\right)+\overline{dW}\right]dx_1 dt=\overline{dA} \quad (1)$$

The internal force and moment vectors F_B and M_B, and linear and angular momentum vectors P_B and H_B are introduced as:

$$\begin{aligned} F_B &= \left(\frac{\partial U}{\partial g}\right)^T, M_B = \left(\frac{\partial U}{\partial k}\right)^T \\ P_B &= \left(\frac{\partial K}{\partial V_B}\right)^T, H_B = \left(\frac{\partial K}{\partial \Omega_B}\right)^T \end{aligned} \quad (2)$$

Where F_B and M_B are the internal force and moment vectors and P_B and H_B are the linear and angular momentum vectors measured in the deformed coordinated frame '*B*'. With the above equations, Equation (1) can be written as:

$$\int_{t_1}^{t_2}\int_{)}^{R}\left[dV_B^{*T}P_B+d\Omega_B^{*T}H_B-dg_B^{*T}F_B-dk_B^{*T}M_B\right]dx_1 dt=dA \quad (3)$$

Where the superscript * means that V_B*, $?_B$*, *?** and *?** satisfy the geometrically exact beam equations given in Reference [2]. To obtain a mixed formulation, Shang [4] adopted Lagrange's multipliers to enforce satisfaction of the geometrically exact kinematical relations. Manipulating the equations properly, we obtain the variational formulation based on exact intrinsic equations for moving beams in the hub rotating frame '*a*' as:

$$\int_{t_1}^{t_2} d\Pi_a dt = 0 \quad (4)$$

Complete expressions resulting from Equation (4) can be found in Reference [4]. Discretizing Equation (4) in a spatial domain into *N* finite elements, the above equation can be reduced to the following:

$$\int_{t\cdot}^{t_2}\sum_{i=1}^{N} d\Pi_i dt = 0 \quad (5)$$

This results in a set of nonlinear governing equation as follows:

$$F_S\left(X,\dot{X}\right)-F_L=0 \quad (6)$$

Where F_S is a structural operator, F_L is an external load operator, and X is the unknown structural state variable vector organized as follows:

$$X = \left[\hat{F}_1^T \hat{M}_1^T u_1^T q_1^T F_1^T M_1^T P_1^T H_1^T .....u_N^T q_N^T F_N^T M_N^T P_N^T H_N^T \hat{u}_{N+1}^T \hat{q}_{N+1}^T\right]^T \quad (7)$$

Where '*u*' is the displacement vector in the frame '*a*' and '*?*' is the rotation vector expressed in terms of the Rodrigues parameters. The hatted terms in the above expression are the boundary values of the corresponding quantities that depend on the boundary conditions. The time derivative of the unknown vector *X* is calculated based on the variables during the previous two time steps, by using 2nd order backward Euler method. Newton-Raphson method is used to solve the nonlinear governing equations (Equation 6). This structural model can be coupled with an appropriate aerodynamic model through the external load operator, F_L. The unknown vector *X* is modified slightly when considering an articulated rotor instead of a hingeless rotor.

Equation 6 is a set of first-order ordinary differential equations. These equations are integrated in time using a second-order backward Euler method. The problem is then converted to the solution of a set of nonlinear algebraic equations of the form:

$$F_S\left(X^n\right) - F_L = 0 \quad (8)$$

Where X^n is the unknown structural vector at time step *n*. Newton method is used to solve the above nonlinear algebraic equations.

3. Validation of the exact beam model

To validate the present geometrically exact beam model, few test cases were numerically simulated using a computer program. The results from one such test case are presented below. A rotating beam clamped at the root and with a tip force acting along *a3* direction as shown in Figure 1 is considered. The material properties of this beam are shown in Table 1. The response of the beam is calculated using the present model and compared with results from DYMORE [5]. DYMORE is a finite element based tool for analysis of nonlinear flexible multibody systems developed by Bauchau and co-workers at the Georgia Institute of Technology, Atlanta. Figure 2 and 3 show the comparison of the tip displacements and rotations under the application of a tip force equal to *50sin20t* N. Figure 4 and 5 show the root forces and moments for the case along with the results from DYMORE simulations. The time step size used in both computer simulations was *1e-3* seconds. It can be seen that the two results are nearly identical except for the axial force component at the root, where the difference between the two codes are less than 2%.

4. Prediction of loads in the control system components

The primary objective of the present work is to develop a comprehensive computational structural dynamics (CSD) tool that can be readily coupled with various analyses developed to model the aerodynamic environment of a helicopter rotor. In particular, we are interested in using this combined aeroelastic tool to estimate the loads acting on the components of the control system of the helicopter.

In this work, we model the rotor blade using the geometrically exact beam theory described in Section 2. The components of the control system such as the pitch link, pitch horn, swashplate and servo actuators are modeled as combination rigid and elastic bodies. We then follow a multi-body dynamics approach to systematically couple this control system model with the beam finite element model to obtain a complete blade-control system model. This unified structural model is developed in a modular fashion so that it can then be easily coupled with various aerodynamic and wake models or even CFD.

As a first step, only the pitch horn, pitch link and the rotating swashplate are considered in this work. The pitch horn and the rotating swashplate are modeled as rigid bodies with negligible mass. The pitch link is modeled as a combination of an elastic linear spring and linear viscous damper. The schematic of the rotor blade and control system is shown in Figure 6. The constraints obtained from the multi-body model of the control system are now solved together with the original blade governing equations (Equation 8) to obtain the blade deformation and loads along with the deformation of the elastic pitch link. The loads acting on the pitch link and the rotating swashplate are then calculated from the above solution. In future, we plan to include an elastic model of the servo-actuators and the inertia properties of the rotating and non-rotating swashplates.

5. Numerical results

The properties of the small-scale rotor are given in Table 2. In the present work, the rotor is assumed to be in hover condition in a wind tunnel. The aerodynamic loads in the current study are obtained from the aerodynamic module of CAMRAD [6, 7]. A simple uniform inflow model was chosen to model the effects of the rotor wake. The aerodynamic lift and pitching moment from CAMRAD are shown in Figures 7 and 8. Figure 9 shows the comparison of the steady flapwise deflection between the present model and CAMRAD. The present model predicts a higher flapwise deflection compared to CAMRAD. Figure 10 shows the lead-lag deflection of

the rotor blade. Again, the present model predicts higher lead-lag deflection compared to CAMRAD. Figure 11 shows the pitch link load versus simulation time. The steady pitch link load in this hover condition is about 22.2 N. There is some small non-steady component in pitch link load. However, this can be reduced to zero by introducing some damping in the system. Figure 12 shows the loads acting on the rotating swashplate along the 3 axes. Since the pitch link connected to the rotating swashplate is almost vertical, the z-component of the swashplate load is the dominant component and is nearly equal to 22 N. In this simulation only one blade is considered. For a 4-bladed rotor, the steady loads acting on the rotating swashplate will be increased a factor of 4.

Currently, we are working on validating our numerical results with the results from CAMRAD. In future, we plan to couple this unified structural model with various aerodynamic and wake models and simulate hover and forward flight conditions. Also, work is currently under way to include multibody model of the non-rotating components of the rotor control system such as non-rotating swashplate and servo actuators.

Acknowledgements

This work has been supported by the Korea Aerospace Research Institute under Korean Helicopter Program Dual-Use Component Development Program, funded by the Ministry of Knowledge Economy. This work is also supported by Defense Acquisition Program Administration and Agency for Defense Development under the contract UD070041AD.

References

1. V L Berdichevsky, "Variational-asymptotic method of constructing a theory of shells," *PMM*, Vol. 43, No. 4, 1979, pp. 664-687.
2. D H Hodges, "A mixed variational formulation based on exact intrinsic equations for dynamics of moving beams," *International Journal of Solids and Structures*, Vol. 25, No. 11, 1990.
3. X Shang and D H Hodges, "Aeroelastic stability of composite rotor blades in hover," *Proceedings of the 36th Structures, Structural Dynamics and Materials Conference*, New Orleans, Lousiana, April 10-12, 1995.
4. X Shang, "Aeroelastic stability of composite hingeless rotors with finite state unsteady aerodynamics," Ph.D. dissertation, Georgia Institute of Technology, 1995.

5. O A Bauchau, "DYMORE: User Manual," Available online at: http://www.ae.gatech.edu/people/obauchau/Dwnld/dymore20/DymoreManual.pdf
6. W Johnson, "Rotorcraft dynamics models for a comprehensive analysis," *Proceedings of the 54th Annual Forum of the American Helicopter Society*, Washington DC, May 20-22, 1998.
7. W Johnson, "Rotorcraft aerodynamics models for a comprehensive analysis," *Proceedings of the 54th Annual Forum of the American Helicopter Society*, Washington DC, May 20-22, 1998.

Table 1: Material properties of the test beam

Mass per unit span	0.2 kg/m
I_{xx}	10^{-4} kg.m
I_{yy}	10^{-6} kg.m
I_{zz}	10^{-4} kg.m
K_{11}	10^{6} N
K_{22}	10^{20} N
K_{33}	10^{20} N
K_{44}	50 N.m^2
K_{55}	50 N.m^2
K_{66}	1000 N.m^2

Table 2: Properties of small-scale rotor

Rotor type	Articulated
Rotor radius, R	1.129 m
Number of blades, N_b	4
Rotor speed, ?	199.38 rad/s

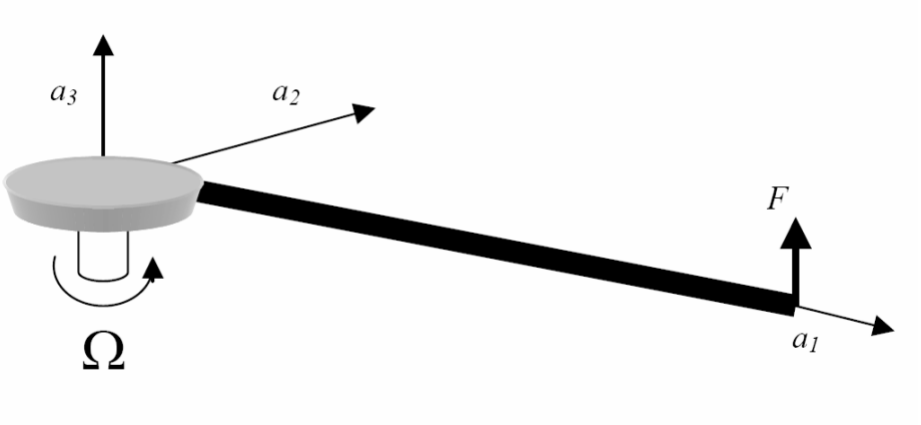

Figure 1: Beam considered for dynamic test

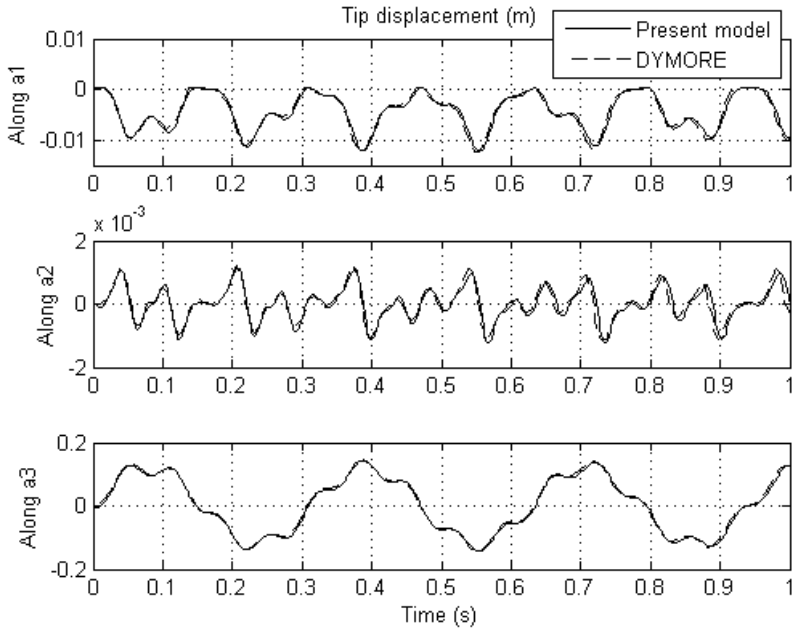

Figure 2: Comparison of tip displacements for test beam

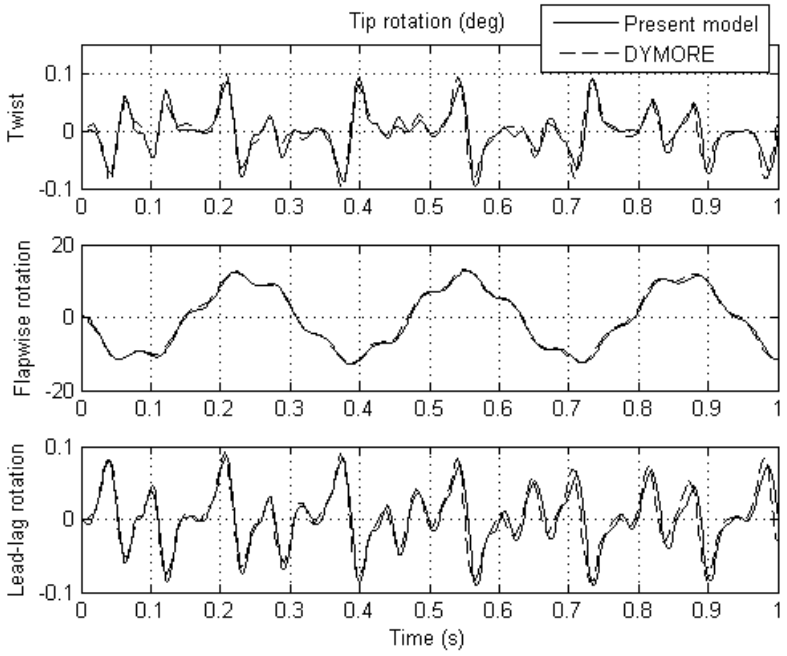

Figure 3: Comparison of tip rotations for test beam

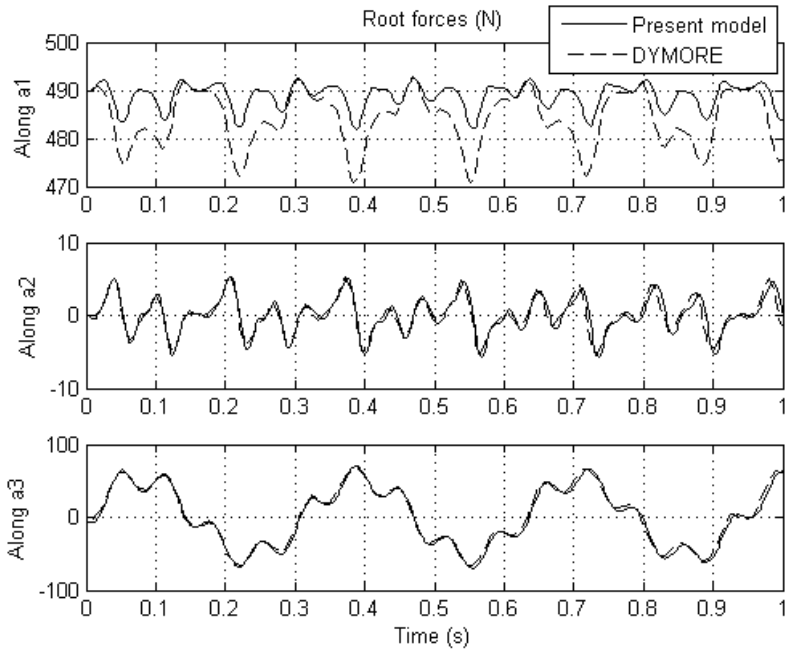

Figure 4: Comparison of root force for test beam

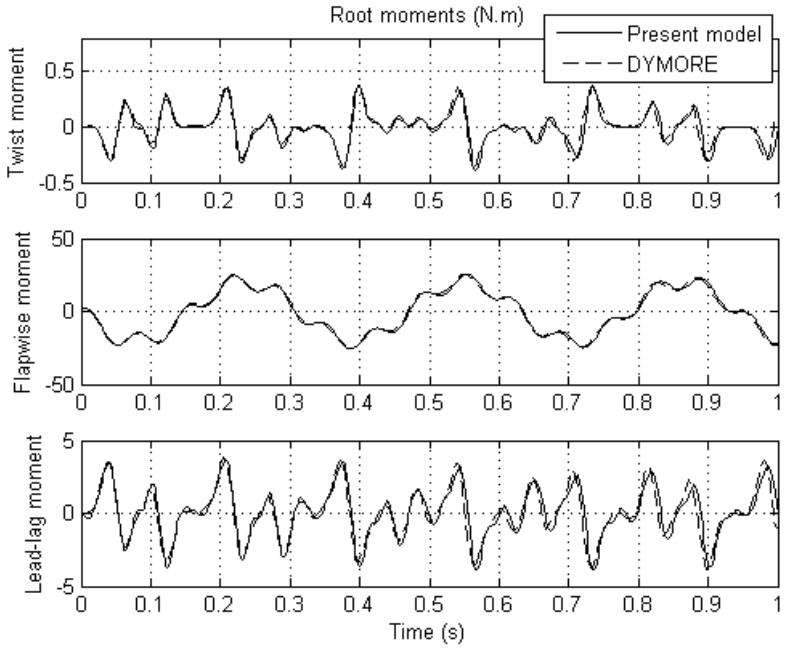

Figure 5: Comparison of root moments for test beam

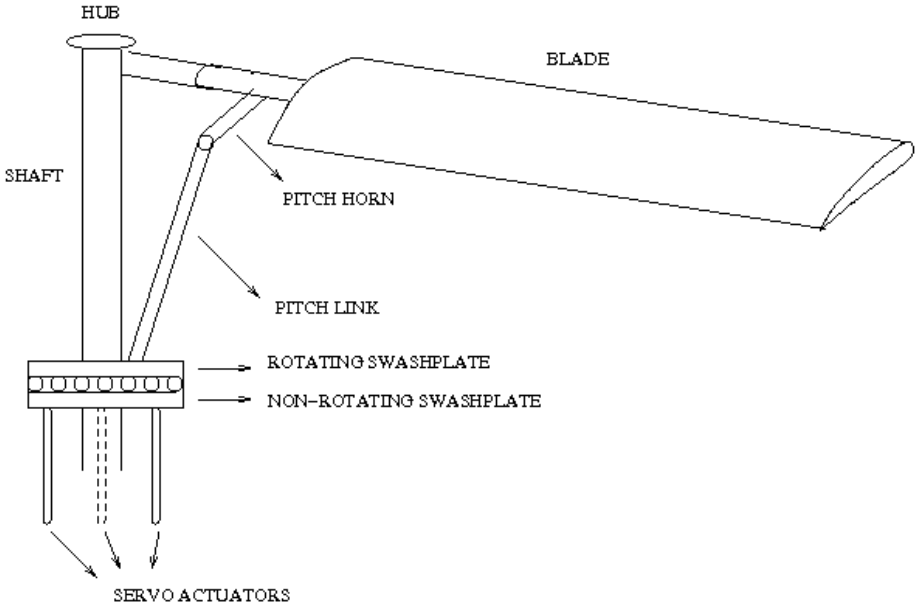

Figure 6: Schematic view of a rotor with control system components

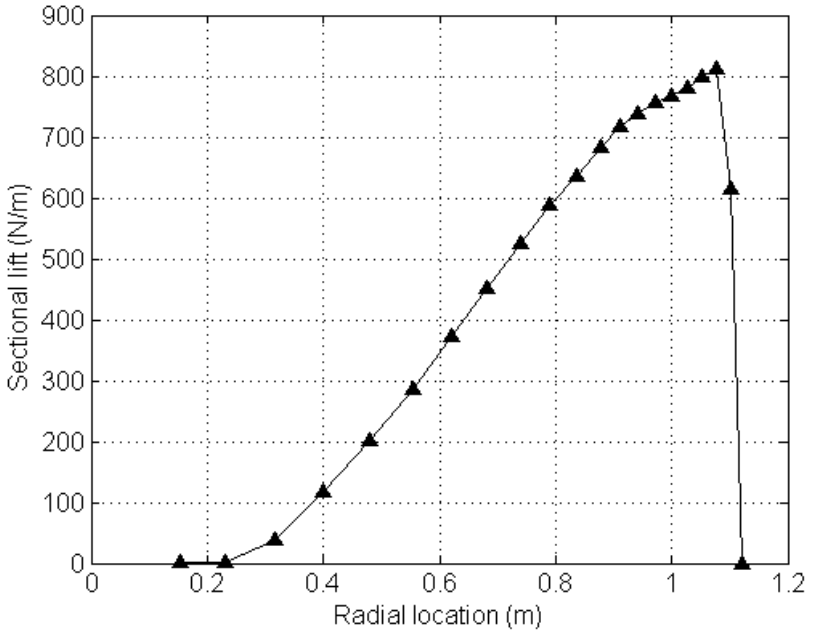

Figure 7: Aerodynamic lift distribution from CAMRAD

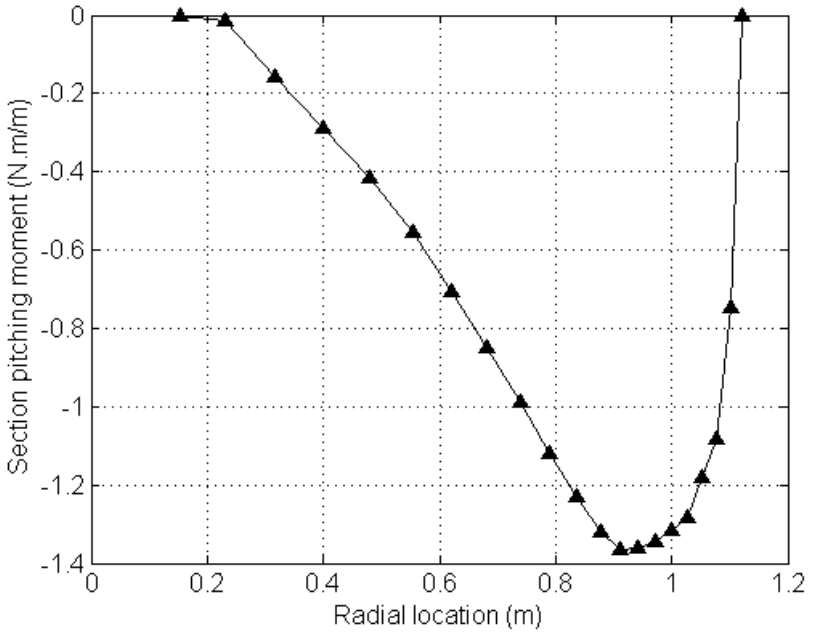

Figure 8: Aerodynamic pitching moment distribution from CAMRAD

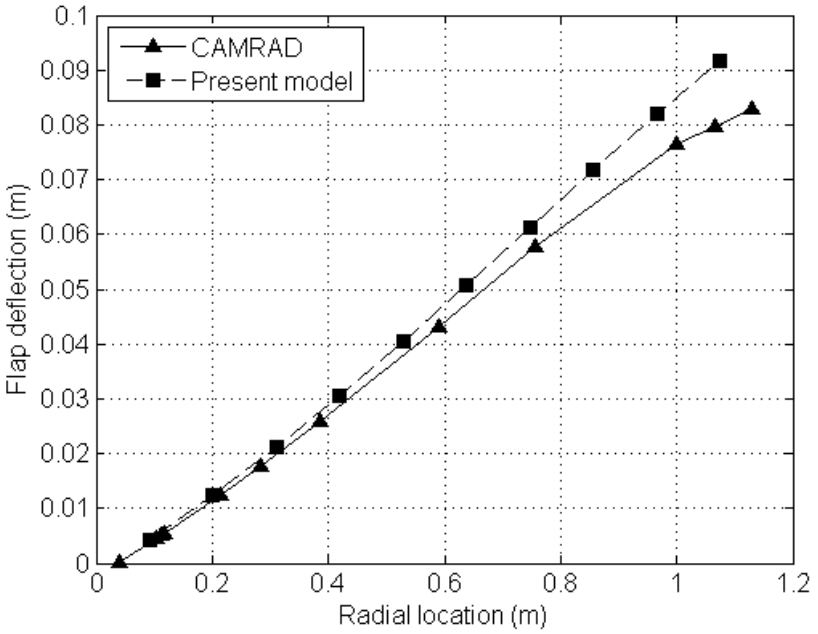

Figure 9: Comparison of flapwise deflection of the rotor in hover

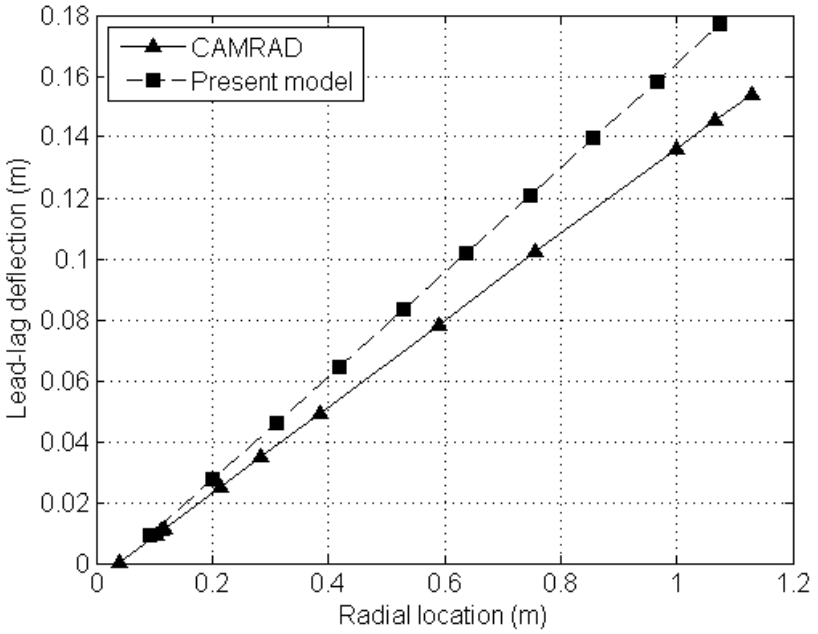

Figure 10: Comparison of lead-lag deflection of the rotor in hover

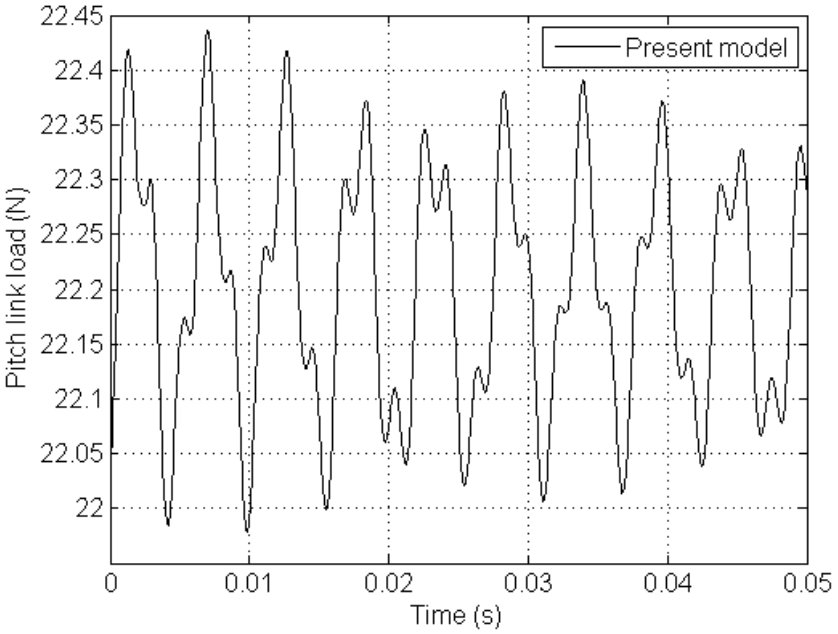

Figure 11: Pitch link load of the rotor in hover

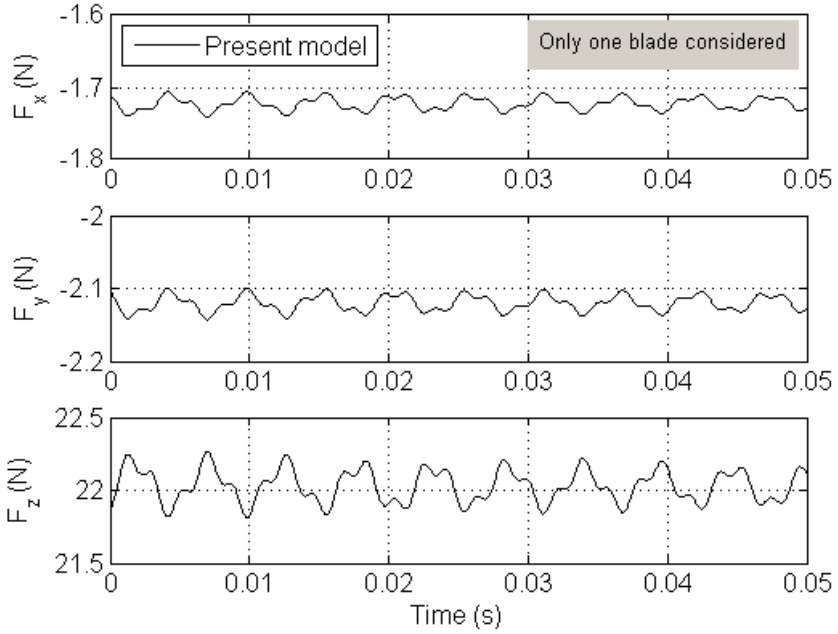

Figure 12: Loads acting on the rotating swashplate of the rotor in hover